INTERNATIONAL JOURNAL OF MARITIME TECHNOLOG

IJMT Vol.5/ Winter 2016 (63-76)

Available online at: http://ijmt.ir/browse.php?a_code=A-10-632-1&sid=1&slc_lang=en

Weakly-compressible SPH and Experimental modeling of periodic wave breaking on a plane slope

Amin Mahmoudi[1*], Habib Hakimzade[2], Mohammad Javad Ketabdari[3], Amir Etemad-Shahidi[4], Nick Cartwright[5], Hassan Abyn[6]

[1] *Assistant Professor, Faculty of Civil Engineering, Persian Gulf University, Bushehr, a_mahmoudi@pgu.ac.ir*
[2] *Professor, Faculty of Civil Engineering, Sahand University of Technology, Tabriz; Hakimzadeh@sut.ac.ir*
[3] *Associate Professor, Faculty of Marine Technology, Amirkabir University of Technology, Tehran, Ketabdar@aut.ac.ir*
[4] *Griffith School of Engineering, Griffith University, Queensland,4222, Australia, a.etemadshahidi@griffith.edu.au*
[5] *Griffith School of Engineering, Griffith University, Queensland, 4222, Australia, n.cartwright@griffith.edu.au*
[6] *Assistant Professor of Naval Architecture, Persian Gulf University, Bushehr, abynhassan@gmail.com*

ARTICLE INFO

Article History:
Received: 8 Feb. 2016
Accepted: 15 Mar. 2016

Keywords:
Experimental Model
Numerical Simulation
weakly compressible smoothed particle hydrodynamics
Wave breaking
large eddy simulation model

ABSTRACT

Breaking waves have ability to transport large quantities of sediment and significant impact on coastal structures morphology. Hence, modeling of wave breaking is an important subject in coastal and marine engineering. In this research, the periodic wave breaking process on a plane slope is studied experimentally and numerically. Laboratory experiments were conducted to record water surface elevation and the wave breaking process. For the current study, a space-averaged Navier–Stokes approach together with laboratory experiments has been deployed to investigate time-dependent wave breaking processes. The developed model is based on the Smoothed Particle Hydrodynamic (SPH) method; a pure Lagrangian approach; capable of handling large deformations at free surface with high accuracy. So, a Weakly Compressible version of the Smoothed Particle Hydrodynamics (WCSPH) method together with a large eddy simulation (LES) approach was used to simulate the wave breaking on a plane slope. The results of numerical simulations were compared both qualitative and quantitative with those of laboratory experiments. Overall, good agreement was found between them. Finally, it is shown that the WCSPH method provides a useful tool to investigate surf zone dynamics.

1. Introduction

The process of wave breaking on beach slopes has attracted much attention among engineers because of its significant impact on costal structures morphology. The potential of breaking waves to displace the sediments and reshape the coastal bathymetry is of great importance in coastal evolution. The breaking waves are categorized as spilling, plunging, and surging, with a gradual transition between each regime [1]. The spilling and plunging breakers are the commonly observed breakers in most natural beaches and the plunging break displays an especially spectacular phenomenon. In order to make solutions for many coastal problems it is needed to clarify the wave breaking process. For many reasons, the study of breaking waves is a very difficult task. For instance, the velocity field during breaking is extremely chaotic and changes rapidly in time. In addition, there is lack of experimental studies on wave breaking because measuring of velocity due to existence of air bubble entrained by the plunging jet is too difficult. Field studies are encountered with limited site access and environmental variability [2], in addition to the previously mentioned limitations. During wave breaking, the shape of the wave deforms rapidly and energy dissipation is high. Since the numerical studies of breaking wave can provide the flow details without scaling and observational constraints, they are becoming more popular in the recent years. Hence, several numerical models have been developed to simulate wave breaking in the surf zone.

The deployment of the fundamental hydrodynamic equations such as the Navier–Stokes (N–S) equations or Reynolds averaged N–S (RANS) equations is the most appropriate way to investigate the breaking

waves [3]. The RANS models have been widely employed and validated in the costal hydrodynamics using the finite difference, finite volume or finite element schemes that are combined with the free surface tracking techniques such as VOF methods.

Lemos [4] simulated a breaking solitary waves and periodic wave breaking on the sloping bed by solving the N–S equations based on SOLC-VOF code coupled with the standard $k-\varepsilon$ turbulence model. Takikawa et al. [5] investigated a plunging breaker over a sloped bed using both the experimental and numerical analyses. Lin and Liu [6] presented spilling and plunging breakers by using an advanced RANS modeling. They found good agreement between the numerical and experimental results. Liu et al. [7] developed a Reynolds-averaged Navier–Stokes (RANS) model to simulate the breaking waves overtopping of a porous structure. For this model, an improved $k-\varepsilon$ model and VOF surface tracking scheme were coupled with their solver. Also, the wave overtopping of a sea wall by solving the N–S equations along with VOF surface tracking scheme and LES turbulence model was modeled by Li et al. [8].

The Lagrangian grid-based methods may not be suitable for analyzing the flows with highly deformed free surface due to grid distribution. On the other hand, the Eulerian grid based methods need a proper interface capturing method that can simulate large and abrupt deformations with fragmentation [9].

Particle methods which are among the mesh-free or gridless methods have been widely deployed in many engineering applications as well as the simulation of flow hydrodynamics. Such techniques represent the state of a system as a set of discrete particles, without a fixed connectivity, followed in a Lagrangian manner. Therefore, particle methods are intrinsically appropriate for the analysis of moving interfaces and free surfaces. Furthermore, fully Lagrangian treatment of particles, resolves the problem associated with grid-based calculations by computing the convection terms without the numerical diffusion.

One of the earliest particle methods, the Smoothed Particle Hydrodynamics (SPH) method was first utilized for astrophysical applications [10,11]. However, it has been extended to model a wide range of engineering applications including elasticity, multiphase-flows and blood simulation for virtual surgery ever since. The method has also been extended and utilized to simulate the incompressible flows by considering the flow as slightly or weakly compressible with a proper equation of state. Run-up and run down of waves on beaches, wave breaking and overtopping on arbitrary structures and interaction between waves and coastal structures are among the applications, but to name a few.

Extensive researches have been conducted, based on the SPH method, to display the feasibility of the approach when dealing with the wave and coastal structures. Shao and Gotoh [12] used ISPH model to the simulation of the solitary wave breaking on a beach. Shao [2], used two-equation $k-\varepsilon$ turbulence model coupled with the incompressible SPH method to examine the spilling and plunging cnoidal wave breaking over a slope. Shao [13] simulated the wave breaking and overtopping over sea wall by ISPH together with $k-\varepsilon$ model. Shao and Changming [3] devised a 2D SPH–LES model applicable to a cnoidal wave breaking and plunging over a mild slope. Khayyer et al. [9] proposed Corrected ISPH (CISPH) method and its application to the breaking and post-breaking of solitary waves on a plane slope.

The turbulence modeling has been of major concern in the study of wave breaking. This paper is intended to apply the 2-D SPS turbulence model of Gotoh et al. [14] to analyze the wave breaking process on a plane slope. For the current study, a weakly compressible version of the smoothed particle hydrodynamics (WCSPH) method along with a LES approach was used to simulate the wave breaking on a plane slope and the computations were compared with both qualitative and quantitative experimental data.

To the authors' knowledge, simulations of wave breaking on slope have been mostly carried out by ISPH model. Furthermore, capability of the WCSPH method along with a LES approach to simulate periodic breaking waves on slope is not reported yet. Capability of the WCSPH method to simulate wave breaking is only reported for solitary waves. For example, Rogers and Dalrymple [15] employed WCSPH-LES model for the solitary wave breaking on a beach. Ketabdari and Roozbahani [43] simulated the Plunging Breaking Solitary Wave by WCSPH with LES model. Also, Issa and Violeau [16] simulated the Plunging Breaking Solitary Wave by WCSPH with various turbulent models, such as constant eddy-viscosity, mixing length and k- model.

The Periodic breaking waves on a sloping beach have been studied in a series of experimental measurements [17-21]. To the knowledge of authors, it seems that the photographs taken during the laboratory experiments were solely reported for solitary waves [22, 23]. However, in our experimental modeling, the wave propagation and breaking process were recorded with a high speed camera positioned perpendicular to the glass walls of the wave tank. The main aim of present paper is using WCSPH-LES model to investigate numerically the periodic breaking waves and the post-breaking processes on slopes. Moreover, to improve the WCSPH results, the Moving Least Squares (MLS) density filter is implemented in the current study. The numerical model results are then compared with those of the experimental model tests of this research study.

This paper is outlined as follows: The numerical model is given in section 2. Physical model is

described in section 3 followed by the results and discussion in section 4. Finally, summary and conclusion is presented in section 5.

2. The Numerical model

2.1. Governing equations

Employing the SPH particle approach, the governing mass and momentum equations for a turbulent flow are presented in the following Lagrangian form:

$$\frac{1}{\rho}\frac{d\rho}{dt}+\nabla.\vec{u}=0 \tag{1}$$

$$\frac{D\vec{u}}{Dt}=-\frac{1}{\rho}\nabla P+\vec{g}+\upsilon_0\nabla^2\vec{u}+\frac{1}{\rho}\nabla.\vec{\tau} \tag{2}$$

where ρ is the density, t is the time, $\vec{u}$ is the velocity, P is the pressure, g is the gravitational acceleration, υ_0 is the kinematic viscosity of laminar flow and τ is the Reynolds stress.

2.2. The SPH method

Monaghan [24, 25] and Liu [26] described the main features of the used SPH method in detail. This method is based on integral interpolants, and we will only refer here to the representation of the constitutive equations in the SPH notation. The main point is to approximately generate any function A(r) with:

$$A(\vec{r})=\int_{\Omega}A(\vec{r}')W(\vec{r}-\vec{r}',h)dr' \tag{3}$$

where r is the vector position; W is the weighting function or kernel; h is called smoothing length. Using this particle approximation, the following function can be written in discrete notation due to this estimation:

$$A(r)=\sum_b m_b\frac{A_b}{\rho_b}W_{ab} \tag{4}$$

The mass and density are noted by m_b and ρ_b, respectively and $W_{ab}=W(\vec{r}_a-\vec{r}_b,h)$ is the weight function or kernel. SPH kernel approach offers an upside by calculating the derivative of a function analytically. In comparison with a method like finite difference, where the derivatives are calculated from neighboring points using the spacing between them, this method is more accurate [27]. For the irregularly spaced SPH particles, this would be extremely complicated. We can get the derivatives of this interpolation by ordinary differentiation.

$$\nabla A(r)=\sum_b m_b\frac{A_b}{\rho_b}\nabla W_{ab} \tag{5}$$

In the SPH, by using an analytical kernel function, the motion of each particle is computed through interactions with the neighboring particles. All terms in the N–S equations during the fluid flow, are formulated by particle interaction models and the need for a grid is obviated [2]. SPH particles move in a Lagrangian coordinates and the advection in N–S equations is directly calculated by the particle motion without the numerical diffusion. Each particle can carry a mass *m*, velocity **u** and other properties would vary upon condition. The basic SPH formulations included in this study are summarized as follows [24].

In a standard SPH formulation, the fluid is considered to be compressible, so the fluid pressure can be specified by using an equation of state instead of solving another differential equation. Changes in the fluid density are calculated as:

$$\frac{d\rho_a}{dt}=\sum_b m_b u_{ab}\nabla_a W_{ab} \tag{6}$$

instead of using a weighted summation of mass terms [24], since it is known to result in an artificial density decrease near fluid interfaces.

As explained above, in the standard SPH formulation the fluid is considered as a weakly compressible fluid. Hence, by using an equation of state for specifying fluid pressure, the equation will be simplified and solved rapidly: in contrast to an equation such as the Poissons equation. The pressure and density formulation represented below is the Tait's equation of state [25]:

$$P=B\left[\left(\frac{\rho}{\rho_0}\right)^{\gamma}-1\right] \tag{7}$$

where γ is 7, B is $c_0^2\rho_0/\gamma$, ρ_0 is 1000 kg/m^3 the reference density, and c_0 is $c(\rho_0)$, the speed of sound at the reference density. The pressure gradient term in the symmetrical form is

$$-\frac{1}{\rho}\nabla P=-\sum_b m_b\left(\frac{P_a}{\rho_a^2}+\frac{P_b}{\rho_b^2}\right)\nabla_a W_{ab} \tag{8}$$

The laminar stress term simplifies to [28, 29]:

$$(\upsilon_0\nabla^2\vec{u})=\sum_b m_b\left(\frac{4\upsilon_0\vec{r}_{ab}\nabla_a W_{ab}}{(\rho_a+\rho_b)|\vec{r}_{ab}|^2}\right)\vec{u}_{ab} \tag{9}$$

where $\vec{r}_{ab}=\vec{r}_a-\vec{r}_b$, $\vec{u}_{ab}=\vec{u}_a-\vec{u}_b$; being $\vec{r}_k$ and $\vec{u}_k$ the position and the velocity corresponding to particle *k* (*a* or *b*) and υ_0 is the kinetic viscosity of laminar flow ($1\times10^{-6}m^2/s$).

SPS was used to represent the effects of turbulence in Sub-Particle *S*cales [30]. This model increases the accuracy of SPH, due to the fact that it preferably predicts the natural action better than the classical artificial viscosity given by Monaghan [24]. Ketabdari and Roozbahani [43] simulated the Plunging Breaking Wave by WCSPH with artificial viscosity and SPS models to consider the accuracy of WCSPH with artificial viscosity and SPS models. The results of overturning motion of a regular wave obtained by the standard WCSPH (with artificial viscosity) model with $\alpha=0.01$, the WCSPH-SPS model, and the

boundary element method (BEM) of Vinje and Brevig [44] at different time instants were compared. Comparisons between the results of these models and those of the base model [44] confirm that the WCSPH-SPS model is a powerful tool for simulating complicated turbulent free surfaces. Then in present numerical model, we used WCSPH‐SPS model.

The eddy viscosity assumption is often deployed to model the SPS stress tensor as follow:

$$\frac{\tau_{ij}}{\bar{\rho}} = 2\upsilon_t \tilde{S}_{ij} - \frac{2}{3}\tilde{S}_{kk}\delta_{ij} - \frac{2}{3}C_I \Delta^2 \delta_{ij}\left|\tilde{S}_{ij}\right|^2 \tag{10}$$

in which, τ_{ij} is the sub-particle stress tensor, $\upsilon_t = (C_s.\Delta l)^2.|\bar{S}|$ is the turbulence eddy viscosity, C_S is the Smagorinsky constant, Δl is the spacing between particles $|\bar{S}| = (2\bar{S}_{ij}\bar{S}_{ij})^{0.5}$ and $\bar{S}_{ij}$ the element of SPS strain tensor. Therefore, the momentum conservation equation can be written in SPH notation as [27]:

$$\begin{aligned}\frac{D\vec{u}_a}{Dt} &= \sum_b m_b\left(-\frac{P_a}{\rho_a^2} - \frac{P_b}{\rho_b^2} + \frac{\tau_a}{\rho_a^2} + \frac{\tau_b}{\rho_b^2}\right)\nabla_a W_{ab} \\ &+ \sum_b m_b\left(\frac{4\upsilon_0 \vec{r}_{ab}.\nabla_a W_{ab}}{(\rho_a + \rho_b)|\vec{r}_{ab}|^2}\right)\vec{u}_{ab} + g\end{aligned} \tag{11}$$

Kernel function has a significant role in SPH method, and for analytical particles, it demarcates the affected area. In this study, the Quintic function, which is generally employed and proposed by Wendland [31], is used:

$$W(r,h) = \alpha_d\left(1-\frac{R}{2}\right)^4(2R+1) \quad 0 \le R \le 2 \tag{12}$$

Where α_d is $7/4\pi h^2$ in 2D, $21/16\pi h^3$ in 3D and $R = r/h$.

In this research, the Predictor-Corrector algorithm described by Monaghan [32] was used in numerical simulations with a time step $\Delta t = 5\times10^{-5}$ s. This time step is small enough to satisfy the Courant condition and to control the stability of force and viscous terms [24].

Despite dynamics results from SPH simulations are realistic in general, large fluctuations can be observed in the pressure field of the particles. To overcome this problem and reduce the fluctuations, several methods have been developed to correct the kernel [33-35] and develop an incompressible solver. Putting a filter to the density of the particles and modifying density of them, is one of the simplest methods [36]. In the present study, we used the Moving Least Squares (MLS) approach which is introduced first by Dilts [37]. More details of the SPH model can be found in [27].

2.2.1. Boundaries

Free surfaces can always be easily recognized by particles in the SPH model. The particle density on the free surface drops abruptly because there is no particle in the outer region of the free surface. This criterion for defining the free surface is very simple and stable even under the plunging and splashing conditions [38]. If the absolute value of the difference between the particle density and reference density exceeds $0.01\rho_0$, then a particle can be regarded as a surface particle.

In this modeling, the boundary is described by a set of discrete boundary particles. Fixed solid boundaries such as the sea bottom and a plane slope are simulated by Repulsive boundary conditions. To assure that a water particle never passes a solid boundary, Monaghan [25] developed this boundary condition. Here, similar to inter-molecular forces, the particles in the boundary exert central forces to the fluid particles. Lennard-Jones potential expresses the force per unit of mass for a boundary particle and a fluid particle separated a distance of *r*. By applying an interpolation method, Monaghan and Kos [39] modified this method and minimized the inter-spacing effect of the boundary particles on the repulsion force of the wall. Later on, Rogers and Dalrymple [40] improved the normal force experienced by a water particle. In this study, we use their modified approach. Following this approach, the force $\vec{f}$ experienced by an FP (fluid particles) acting normal to the wall, was modified by Rogers and Dalrymple (2008):

$$\vec{f} = \vec{n}R(\psi)P(\xi)\varepsilon(z,u_\perp) \tag{13}$$

where $\vec{n}$ is the normal of the solid wall. The distance ψ is the perpendicular distance of the particle from the wall, while ξ is the projection of interpolation location on to the chord joining the two adjacent boundary particles and $u_\perp = (\vec{v}_{FP} - \vec{v}_{BP})$. $\vec{n}$ is the velocity of the FP projected onto the normal. The repulsion function, $R(\psi)$, is evaluated in terms of the normalized distance from the wall, $q_n = \psi/2h$, as

$$R(\psi) = A\frac{1}{\sqrt{q_n}}(1-q_n) \tag{14}$$

where the coefficient A is

$$A = \frac{1}{h}0.01c_a^2 \tag{15}$$

The function $P(\xi)$ is chosen so that an FP experiences a constant repulsive force as it travels parallel to the wall

$$P(\xi) = \frac{1}{2}\left(1+\cos\left(\frac{2\pi\xi}{\Delta b}\right)\right) \quad or \quad P(\xi) = \left(1-\frac{\xi}{\Delta b}\right) \tag{16}$$

where Δb is the distance between any two adjacent BPs (boundary particles). Finally, the function $\varepsilon(z,u_\perp)$ was modified from Monaghan and Kos (1999) and adjusts the magnitude of the force according to the local water depth and velocity of the FP normal to the boundary

$$\varepsilon(z,u_\perp)=\varepsilon(z)+\varepsilon(u_\perp) \tag{17}$$

where

$$\varepsilon(z)=\begin{cases}0.02 & z\geq 0\\ |z/h_0|+0.02 & 0\succ z\succ -h_0\\ 1 & |z/h_0|\succ 1\end{cases} \tag{18}$$

and

$$\varepsilon(u_\perp)=\begin{cases}0 & u_\perp\succ 0\\ |40u_\perp|/c_0 & |40u_\perp|\prec c_0\\ 1 & |40u_\perp|\succ c_0\end{cases} \tag{19}$$

z is the elevation above the local still-water level h_o.

The system of normal requires each BP to know the coordinates of its adjacent BPs. In a two-dimensional situation (Figure 1), the BP a is surrounded by BPs n_1 and n_2 so that the tangential vector is given by $\vec{t}=(\vec{r}_{n2}-\vec{r}_{n1})/|\vec{r}_{n2}-\vec{r}_{n1}|$ and the normal is calculated using $\vec{n}.\vec{t}=0$.

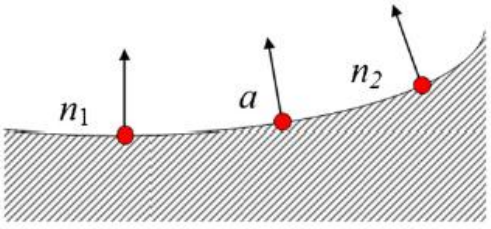

Figure 1. Location of adjacent boundary particles for RBCs

The upstream open boundary is the incident wave boundary. This boundary is modeled by a numerical wave maker composed of wall particles. During the computation, the wave maker moves periodically and its frequency and amplitude are adequately adjusted until the desired incident wave profile is obtained. Following Mahmoudi et al. [45], the wave maker is designed to be able to produce an incident wave and meanwhile, absorb reflected waves from the downstream.

Base on linear wave-making theory, a paddle wavemaker with simple harmonic motion with amplitude, A_p and angular frequency ω, that the equilibrium position is origin, can generate a linear wave in a flume, and the wave surface η is

$$\eta=A_pC_0\cos(kx-\omega t)+A_p\sum_{n=1}^{\infty}C_ne^{-kx}\sin(\omega t) \tag{20}$$

where

$$C_0=\frac{2[\cosh(2kh)-1]}{\sinh(2kh)+2kh} \tag{21}$$

$$C_n=\frac{2[\cos(2k_nh)-1]}{\sin(2k_nh)+2k_nh} \tag{22}$$

where h is water depth, x is the distance from wavemaker. In this equation, the wave number k satisfies the following formula,

$$kg.\tanh(kd)-\omega^2=0 \tag{23}$$

and k_n is the nth root of the equation below,

$$k_ng.\tan(k_nd)+\omega^2=0 \tag{24}$$

To absorb the secondary reflecting waves from the wave maker, an additional wave maker displacement X_a is added on the original displacement X_p. Then, the displacement of the absorbing wavemaker is

$$X=X_p+X_a=A_p\sin(\omega t)+A_a\sin(\omega t+\varphi) \tag{25}$$

The final expression of the velocity of the paddle can be obtained as

$$u(t)=\frac{dX}{dt}=\frac{\omega}{C_0}[2\eta_p-\eta_m+D.X(t)] \tag{26}$$

where φ is phase difference, η_p is the wave surface generated by X_p, η_m is the wave surface that measured in front of the wave maker, and $D=\sum_{n=1}^{\infty}C_n$ [47].

To absorb the wave reflection from the wall at the end of the open channel, an exponential damping zone is placed over a distance of at least a wavelength. In the damping zone, the velocity of fluid particles will be damped as

$$U=U_0[1-\exp(-\alpha(\delta x_0-(x-x_0)))] \tag{27}$$

where U is fluid velocity, α is a coefficient, equal to 2.0; δx_0 is the damping zone length, x_0 is the damping zone starting point, $x_0=L-\delta x_0$ and L is the channel length [46].

2.2.2. Initial conditions

Fluid particles were initially placed on a Cartesian grid with dx=dz=0.005 m and zero initial velocity. The particles are assigned an initial density ρ_0 that is needed to be adjusted to yield the correct hydrostatic pressure when the pressure is calculated from the equation of state (7). Considering the gravity acting in the negative z-direction, the density of a particle was given by

$$\rho=\rho_0\left(1+\frac{\rho_0g(H-z)}{B}\right)^{\frac{1}{\gamma}} \tag{28}$$

Where H is the depth of the tank and z is the distance from the particle to the bottom [41]. The initial conditions were designed to fit the experimental conditions. The computational system consists of a wave maker at one end of the tank and a sloping plane at the other one. The computational tank was 8 m long and 0.5 m high (see Fig2). Using this initial configuration, the total number of particles in the numerical experiment was 27,163, with the particles spaces being set to be 0.005 in two directions.

3. Physical modeling

3.1. Experimental set-up

Experiments were conducted in the Hydraulics Laboratory, School of Engineering, Griffith University Gold Coast Campus. The experimental set-up is depicted in Figure 2. The wave tank is 8 m long, 80 cm high and 50 cm wide. A 1:10 slope was placed at a side of the flume. The vertical direction is defined as z -axis. The x-axis is direction for wave propagation. The slope is located at X =2.5 m from the wave maker. Considering a relatively short flume in length employed in this research work, in order to overcome the effect of reflection from the sloping side, depending on the fluctuation in the flume, regular waves were generated on the plane slope for 10‑20 s.

In the experiments, ten wave probes were used to measure the wave profile. The location of wave gauges is shown in Table 1.

The wave propagation and breaking process were recorded with the high speed camera positioned perpendicular to the glass walls of the wave tank. A sketch of the arrangement of the equipment is presented in Figure 2. The recording area were illuminated with two 500W lamps, were placed nearby the high-speed camera. A translucent panel was placed on the far side of the wave tank to provide a uniformly illuminated background. The regular wave was used as the incident wave in the experiment. The wave periods were from 1.14 to 3.42 sec, wave heights from 5.2 cm to 10.2 cm, and the water depth was 0.2 m.

4. Results and Discussion

As mentioned above, the breaking type is generally classified as the spilling, plunging and surging. Classification of wave breaking may be correlated to the surf similarity parameter [42]:

$$\xi_0 = \tan\beta \left(\frac{H_0}{L_0} \right)^{-\frac{1}{2}} \tag{29}$$

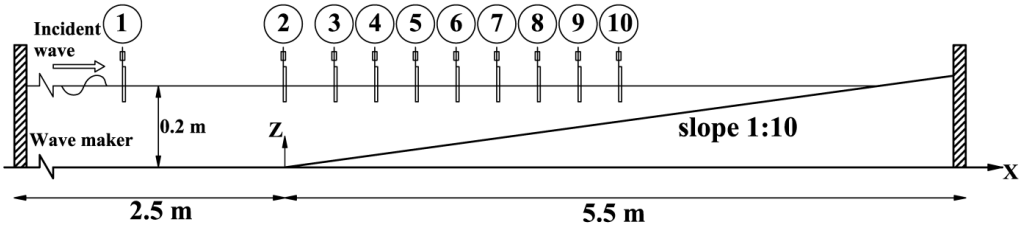

Figure 2. Schematic diagram of experimental set-up

Table 1. Location of wave gages

Wave gage No.	1	2	3	4	5	6	7	8	9	10
X (m)	-1.5	0	0.25	0.45	0.65	0.85	1.05	1.25	1.45	1.65

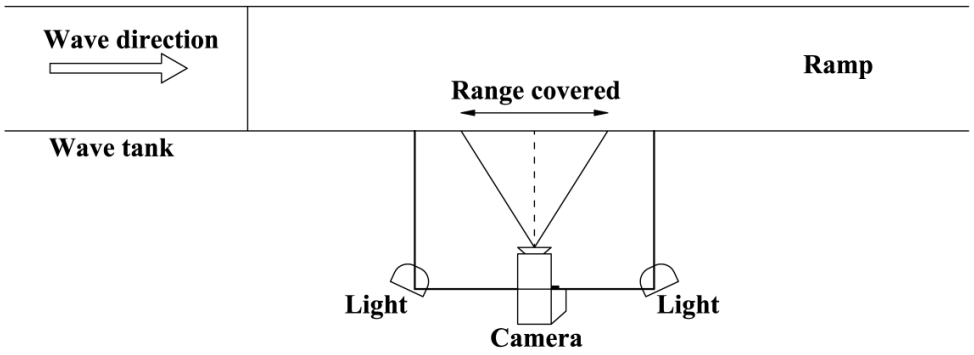

Figure 3. Sketch of the experimental arrangement for side view recording

Table 2. Physical conditions of simulation cases

Simulation case	Wave height (m)	Wave period (sec)	surf similarity	Breaking type
Case I	0.0664	1.8	0.589	Plunging
Case II	0.0758	2.7	0.7037	Plunging
Case III	0.07	1.14	0.4342	Spilling

Where $\tan\beta$ is the slope, H_0 is the deep-water wave height and L_0 is the deep-water wave length

Wave breaking type criterions are then introduced by: (a) surging ($\xi_0 \geq 3.3$); (b) plunging ($0.5 \prec \xi_0 \prec 3.3$) and (c) spilling ($\xi_0 \prec 0.5$) [42].

In the present research, a total number of three cases of periodic wave breaking on the sloping bed were simulated. Among which were two cases of plunging breaking and one case of spilling breaking. The simulation conditions of the plunging breaking cases correspond to those of the present experimental study. The physical conditions of all the mentioned cases are summarized in Table 2. The initial water depth in all three cases was 0.2 m. the initial particle spacing was chosen as dx = 0 .005 m and approximately 27,160 particles were employed in the simulations.

Figure 4 shows the comparison of the numerical and experimental results of wave surface elevation (ζ) under regular wave for the first case. When wave propagates on the slope, it is influenced by shoaling as the depth of water decreases. Hence, the wave profile becomes unsymmetrical, the transmitted wave height increase, the wave crest becomes steeper and eventually it breaks. However, some discrepancies are found in all cases considered here for the maximum and minimum water surface elevations. Then, the developed model predicts the minimum water surface elevation and maximum water surface elevation, slightly underestimated and slightly overestimates, respectively. In general, these wave surface elevations under regular wave are shown that the numerical results agree well with the experimental data both phase wise and amplitude wise, although there are several slight discrepancies between the experimental and numerical wave surface elevations.

When wave propagates on the slope, influenced by shoaling as the depth of water decreases, wave front becomes continuously steeper until the wave breaks. The breaking point is defined as the point where the front face of the wave crest becomes nearly vertical. In other words, the breaking point is defined at the point where the maximum wave height is obtained.

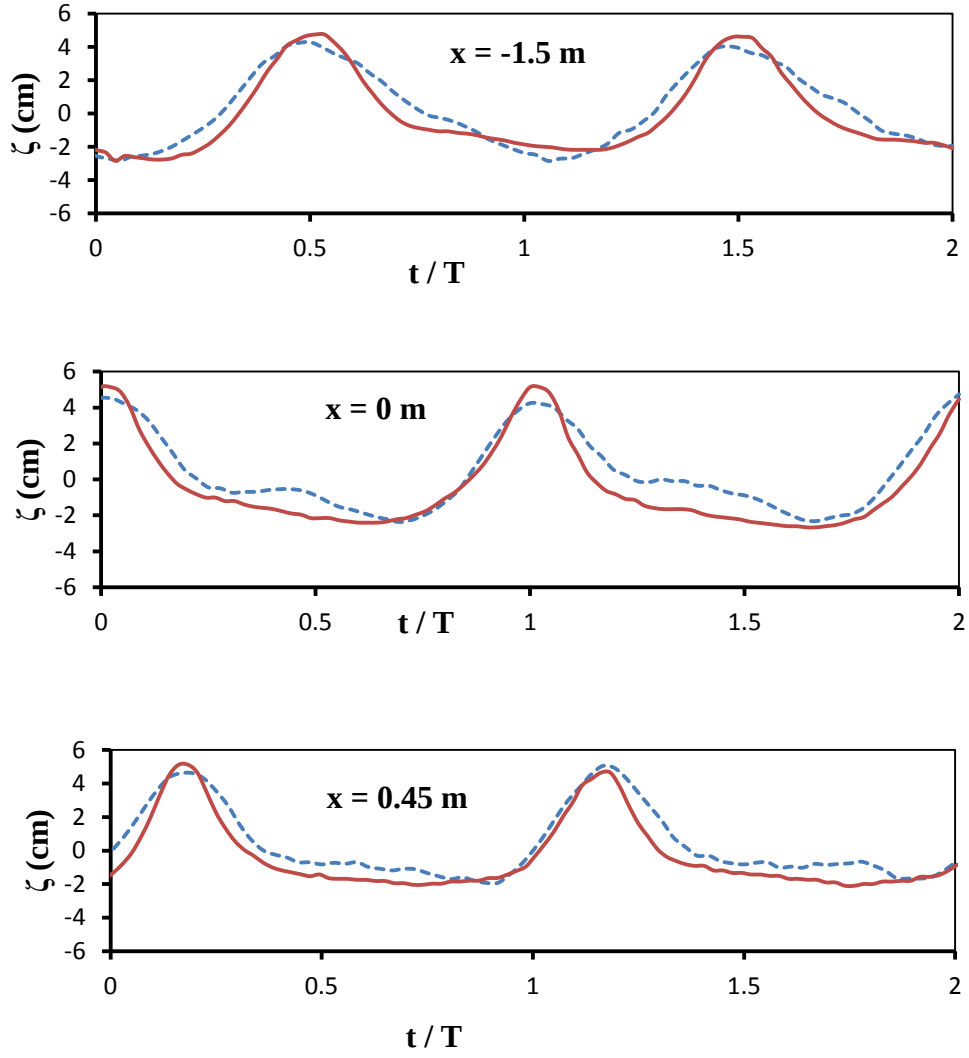

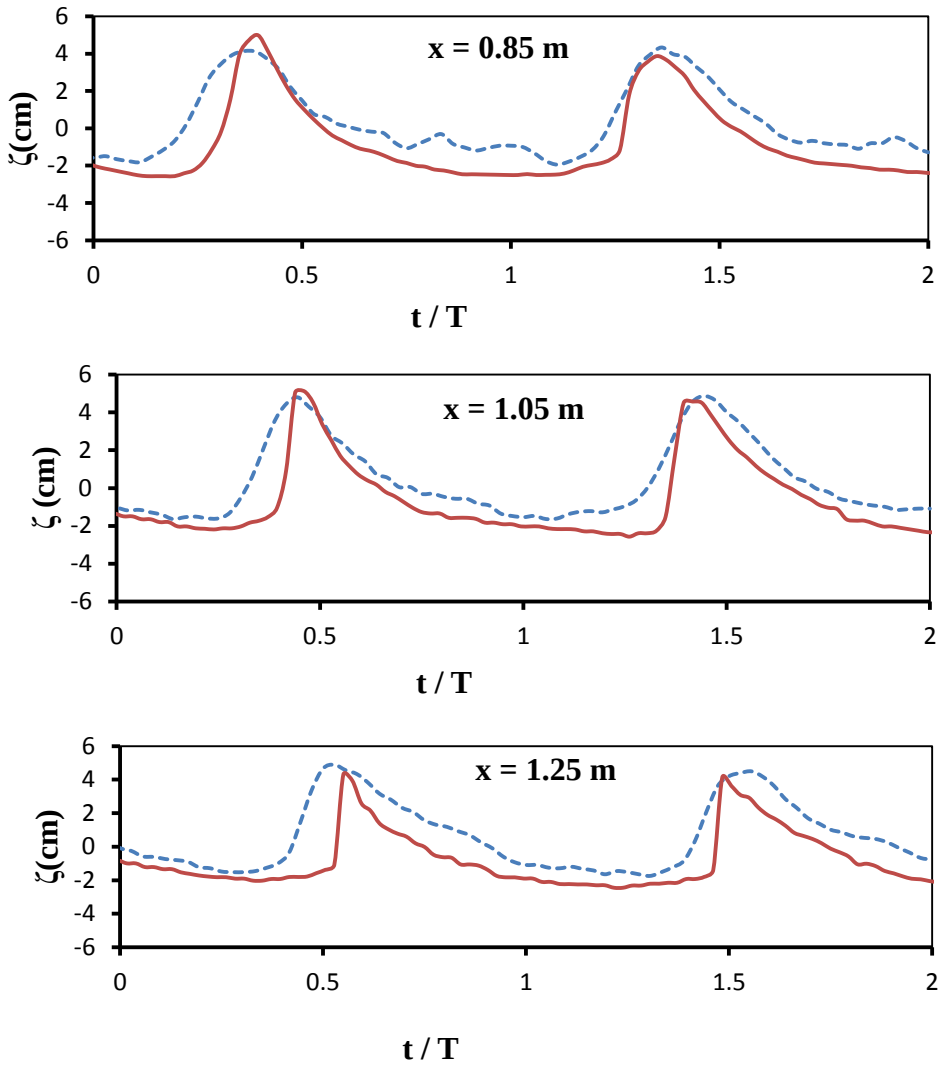

Figure 4. Comparison of the computational and experimental results of the instantaneous water surface elevation versus the normalized time (t/T), case I. Blue dashed line is the experimental data and red solid line are the SPH results

Figure 5 shows a comparison of the variation in wave height H/h_0 for the first case, where h_0 is the offshore water-depth (0.2 m). The laboratory experiments showed a breaking wave height $H_b/h_0 = 0.336$ at $X_b/h_0 = 5.14$ for case I. Ting and Kirby [18] studied a series of experimental measurements for cnoidal wave breaking on a plane slope. They recorded a breaking wave height $H_b/h_0 = 0.406$ for the spilling breaker and $H_b/h_0 = 0.475$ for plunging breaker. Then, the results of present experimental model for breaking criteria are in reasonable agreement with the similar data. In comparison, the SPH modeling predicts a breaking wave height $H_b/h_0 = 0.371$ at $X_b/h_0 = 5.27$ for case I. This shows that a larger wave height is obtained by the WCSPH approach, since it uses particles to track the free surfaces without numerical diffusion.

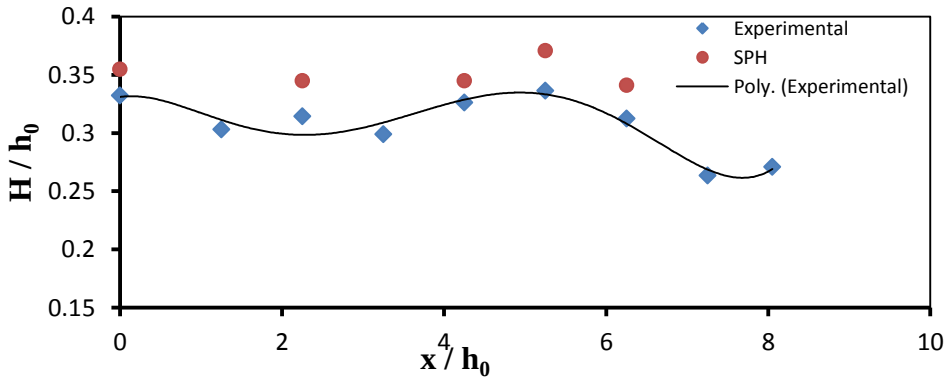

Figure 5. Comparison of variation in wave height during wave propagates on plane slope, case I

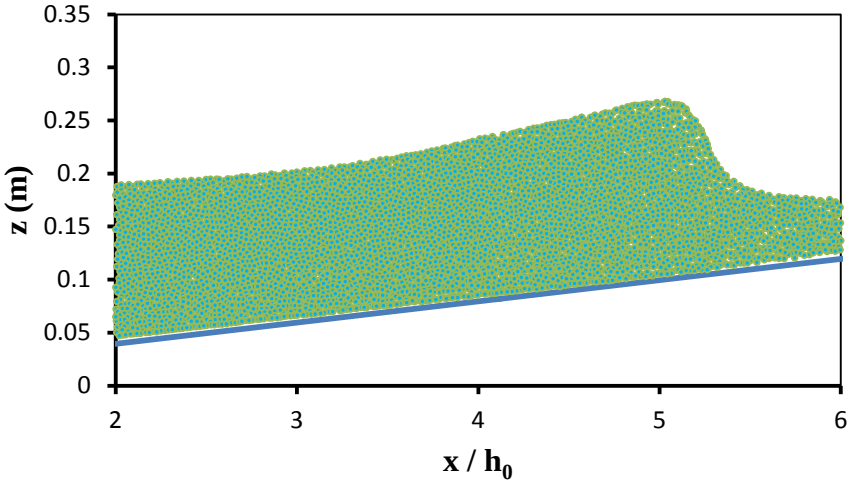

Figure 6. illustrates the WCSPH snapshot of plunging breaking for case I at the breaking point. It shows at $X / h_0 = 5.27$, where the front face of the wave crest becomes nearly vertical

Figure 7 and Figure 9 illustrate the plunging breaking and the splash-up process of a periodic wave with conditions corresponding to the simulation case I and case II, respectively. In the right hand side, the photographs are those taken with the high speed camera during laboratory experiments in the present experimental study, while, the WCSPH results are shown on the left hand side. Qualitative comparison of laboratory photographs with WCSPH results are also shown in Fig 8 and Fig 10 for case I and case II, respectively.

The WCSPH snapshots show qualitatively well agreement to the laboratory photographs. In general, the model was able to simulate the development and impact of the plunging jet with the resulting splash-up process successfully.

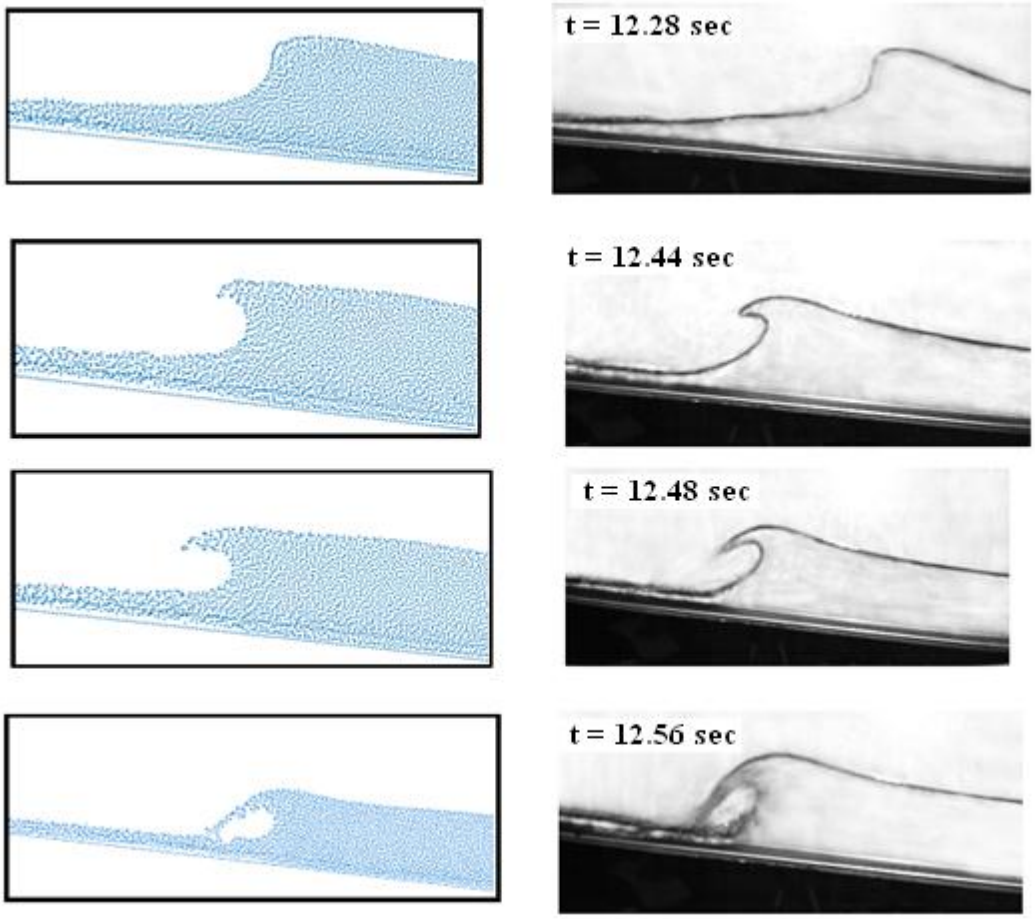

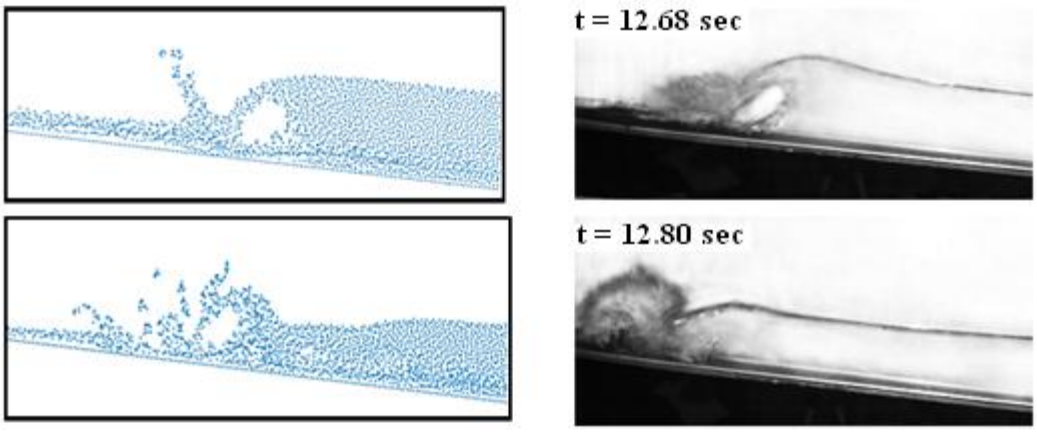

Figure7. Comparison of laboratory photographs (right) with WCSPH (left), case I

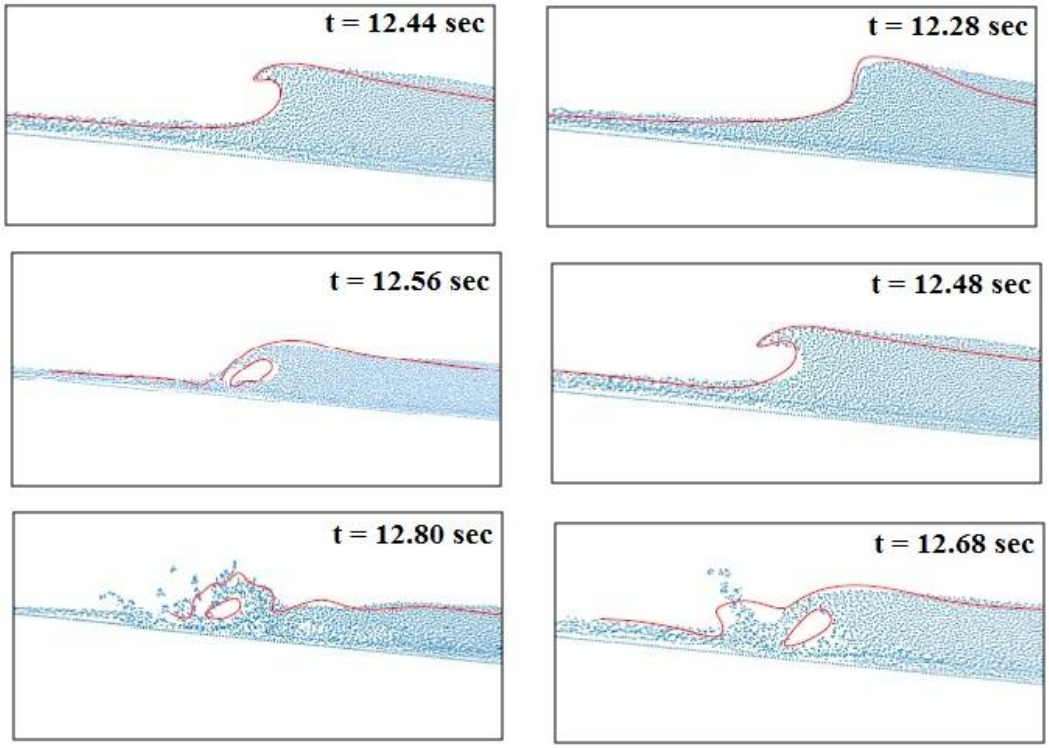

Figure 8. Qualitative comparison of laboratory photographs with WCSPH, case I

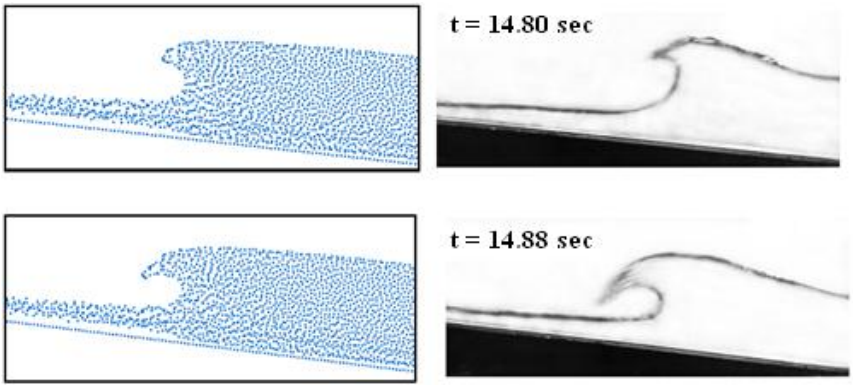

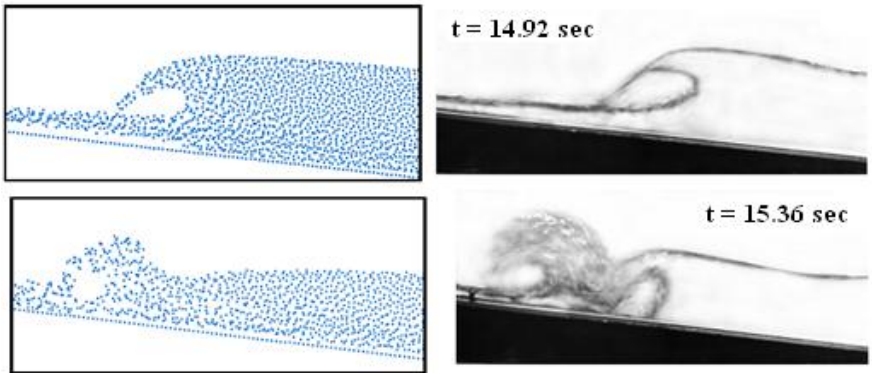

Figure 9. Comparison of laboratory photographs (right) with WCSPH (left), case II

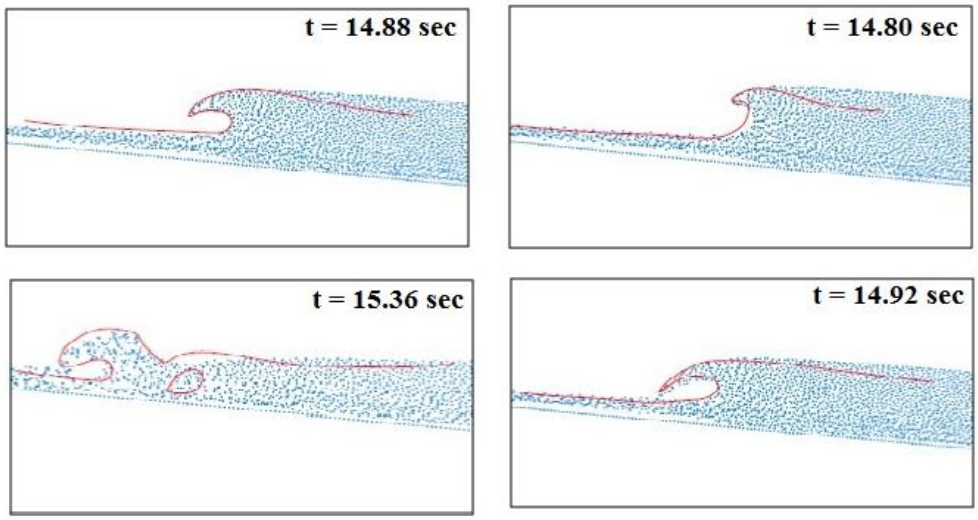

Figure 10. Qualitative comparison of laboratory photographs with WCSPH, case II

Some snapshots of water particles are also shown in Figure 11 for simulation case III. The spilling breaker is a milder wave breaking process, however, the plunging breaker is much more violent. In addition, in spilling breaker the wave keeps its quasi-symmetric form up to the final collapse and the wave height diminished slowly as shown in Figure 11.

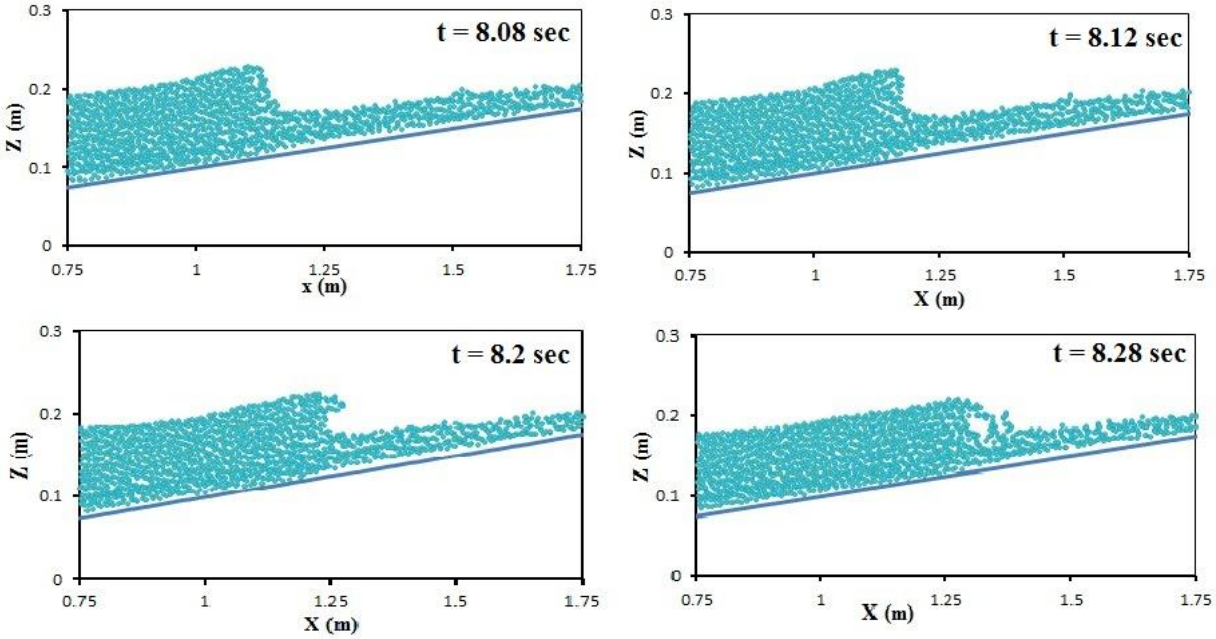

Figure 11. Typical WCSPH snapshots of spilling types of wave breaking, case III

In order to study the influence of particle spacing on the results, the present model was run using different particle spacing. The computed water surface elevations at the three measuring stations were compared with those of the experimental data for two particle spacing in Figure 12. It is shown that a finer model agrees better with the experimental results, the water surface is smoother and the fluctuations of water surface are less. In addition, the present model was also re-run using the finer particle spacing and the results showed that the changes in water surface profile were negligible.

There are some negligible differences between the simulation and the experimental results, although the WCSPH-LES model was able to simulate the plunging breaking waves. In the emergence of numerical errors, the most possible factor behind both the existing differences happens due to completeness deficiency of SPH interpolants. The perfection in mesh free methods refers to the capability of the kernel interpolants to make over a physical field, based on the nodal values. It is similar to the consistency in the finite difference literature [9, 35]. Since, the perfection of the SPH interpolants is not exactly respond here, some numerical errors appear when it comes to the reproduction of highly non-linear velocity fields during the breaking and post-breaking processes.

Simulating this type of flow with a two-phase simulation involving air should increase the quality of the presented results. Nevertheless, when the WCSPH is used to model the details of the highly nonlinear physical processes, implementation of such kind of improvements should be considered.

5. Summary and Conclusion

In this study a weakly compressible version of the smoothed particle hydrodynamics (WCSPH) method together with a large eddy simulation (LES) approach was used to simulate the periodic wave breaking on a plane slope. The simulations are in good agreement with both qualitative and quantitative experimental data. Qualitative comparisons between WCSPH results with the conducted laboratory photographs illustrate the capability of the WCSPH method in the simulation of plunging breaking waves on a plane slope. In addition, it is shown that the WCSPH method provides a useful tool to investigate the surf zone dynamics.

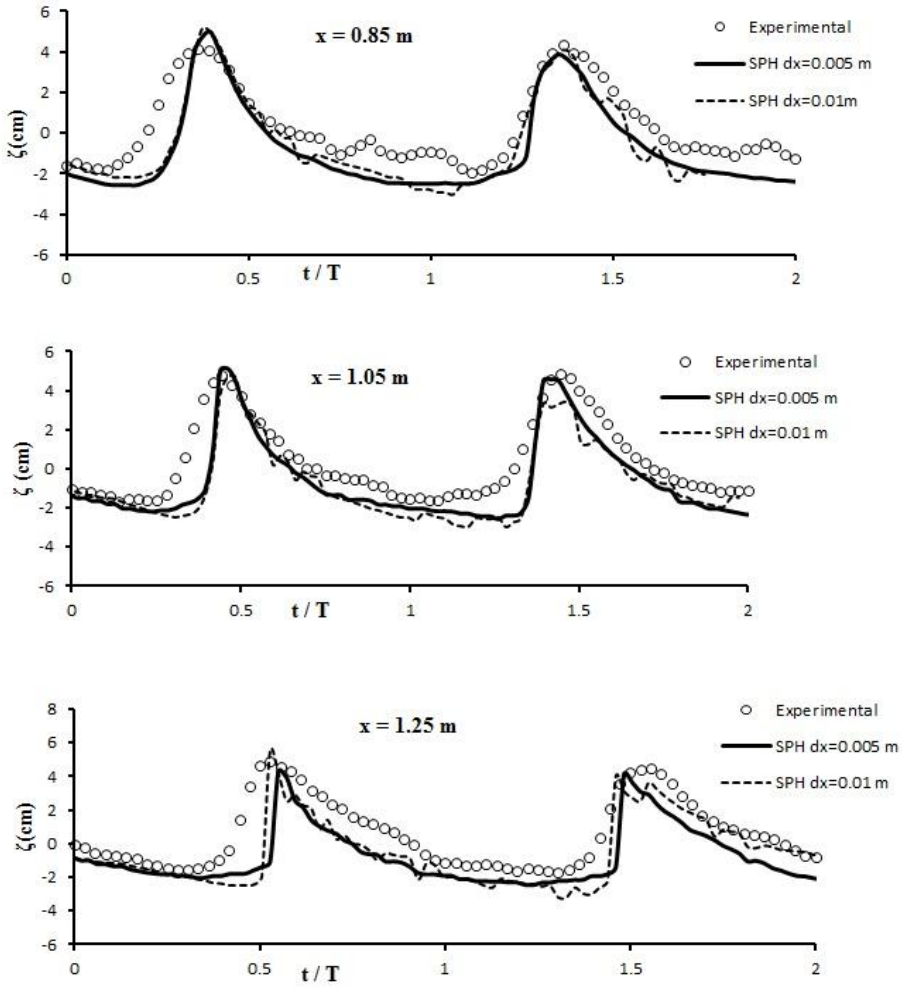

Figure 12. Comparisons of computed water surface elevations using various particle spacing with experimental, case I.

6. ACKNOWLEDGMENTS

The authors would like to acknowledge Dr. C. Crespo, University of Vigo Spain, for his invaluable guidance and advice. The authors also kindly acknowledge Dr. C. Lemckert, the School of Engineering, Griffith University Gold Coast Campus, for giving the opportunity and facilities for doing experimental tests.

7. References

1- Dean, R.G., Dalrymple, R.A., (1991), *Water Wave Mechanics for Engineers and Scientists, Advanced Series on Ocean Engineering*, World Scientific Publication, Singapore.

2- Shao, S.D., (2006), *Simulation of breaking wave by SPH method coupled with* $k-\varepsilon$ *model*, J. Hydraul. Res., 3, 338–349.

3- Shao, S.D., Changming, J.i., (2006), *SPH computation of plunging waves using a 2-D sub particle scale (SPS) turbulence model*, Int. J. Numer. Meth. Fl., 51, 913–936.

4- Lemos, C., (1992), *Wave Breaking, A Numerical Study*, Lecture Notes in Engineering, Springer, Berlin,.

5- Takikawa, K., Yamada F., Matsumoto K.,(1997), *Internal characteristics and numerical analysis of plunging breaker on a slope*, Coast. Eng., 31, 143–161.

6- Lin, P.Z., Liu P.L.F., (1998), *A numerical study of breaking waves in the surf zone*, J. Fluid Mech., 359, 239–264.

7- Liu, P.L.F., Lin P.Z., Chang KA, Sakakiyama T., (1999), *Numerical modelling of wave interaction with porous structures*, J. Waterw. Port Coast. Ocean Eng., 125(6), 322–330.

8- Li, T.Q., Troch, P., Rouck J.D., (2004), *Wave overtopping over a sea dyke* , J. Comput. Phys., 198, 686–726.

9- Khayyer, A., Goth, H., Shao, S.D.,(2008), *Corrected Incompressible SPH method for accurate water-surface tracking in breaking waves*, Coast. Eng., 55, 236–250.

10- Lucy, L.B.,(1977), *A numerical approach to the testing of the fission hypothesis*, Astron. J., 82, 1013–1024.

11- Gingold, R.A., Monaghan, J.J., (1977), *Smoothed particle hydrodynamics: theory and application to non-spherical stars*, Mon. Not. R. Astron. Soc., 181, 375–389.

12- Shao S.D, Gotoh H., (2005), *Turbulence particle models for tracking free surfaces*, J. Hydraul. Res., 43(3), 276–289.

13- Shao S.D., (2006), *Incompressible SPH simulation of wave breaking and overtopping with turbulence modeling*, Int. J. Numer. Meth. Fl., 50, 597–621.

14- Gotoh H, Shibahara T, Sakai T., (2001*), Sub-particle-scale turbulence model for the MPS method Lagrangian flow model for hydraulic engineering*, Comput. Fluid Dyn. J., 4, 339–347.

15- Rogers, B.D., Dalrymple, R.A., (2004), *SPH modeling of breaking waves.* Proc. 29th Intl. Conference on Coastal Engineering, World Scientific Press, pp. 415 – 427.

16- Issa, R., Violeau, D., (2009), *Modelling a Plunging Breaking Solitary Wave with Eddy-Viscosity Turbulent SPH Models*, CMC, vol.8, no.3, pp.151-164.

17- Nadaoka, K., Hino, M., Koyano, Y., (1989), *Structure of the turbulent-flow field under breaking waves in the surf zone*, J. Fluid Mech., 204, 359–387.

18-Ting, F. C. K., Kirby, J. T., (1994), *Observation of undertow and turbulence in a laboratory surf zone*, Coast. Eng., 24, 51–80.

19- Ting, F. C. K., Kirby, J. T., (1995), *Dynamics of surf-zone turbulence in a strong plunging breaker*, Coast. Eng., 24, 177–204.

20- Stansby, P. K., Feng, T., (2005), *Kinematics and depth-integrated terms in surf zone waves from laboratory measurement*, J. Fluid Mech., 529, 279–310.

21- Kimmoun, O., Branger, H., (2007), *A particle image velocimetry investigation on laboratory surf-zone breaking waves over a sloping beach*, J. Fluid Mech., 588, 353–397.

22- Li, Y., (2000), *Tsunamis: Non-breaking and breaking solitary wave run-up.* Rep. KH-R-60, W. M. Keck Laboratory of Hydraulics and Water Resources, California Institute of Technology, Pasadena, CA.

23- Li, Y., Raichlen, F., (2003), *Energy balance model for breaking solitary wave run up*, J. Waterw. Port Coast. Ocean Eng., 129 (2), 47 – 59.

24- Monaghan, J. J.,(1992), *Smoothed Particle Hydrodynamics*, Annu. Rev. Astron. Astr., 30, 543–574.

25- Monaghan, J. J.,(1994), *Simulating free surface flows with SPH*, J. Comput. Phys., 110, 399–406.

26- Liu , G.R.,(2003), *Mesh Free Methods: Moving Beyond the Finite Element Method*, CRC Press, pp.692.

27- Crespo, A.J.C.,(2008), *Application of the Smoothed Particle Hydrodynamics model SPHysics to free-surface hydrodynamic*, PhD Thesis, Universidad de Vigo.

28- Morris, J., Fox, P., and Zhu, Y., (1997), *Modeling low Reynolds number incompressible flows using SPH*, J. Comput. Phys., 136, 214–226.

29- Lo, E. and Shao, S., (2002), *Simulation of near-shore solitary waves mechanics by an incompressible SPH method*, Appl. Ocean Res., 24, 275–286.

30- Dalrymple, R.A., Rogers B.D., (2006), *Numerical modeling of water waves with the SPH method*, Coast. Eng., 53,141 – 147.

31- Wendland, H., (1995), *Piecewiese polynomial, positive definite and compactly supported radial*

functions of minimal degree, Adv. Comput. Math., 4(1), 389– 396.
32- Monaghan, J. J., (1989), *On the Problem of Penetration in Particle Methods,* J. Comput. Phys., 82, 1–15.
33- Randles, P. and Libersky, L., (1996), *Smoothed Particle Hydrodynamics some recent improvements and applications,* Comput. Method Appl. M., 138, 375–408.
34- Bonet, J., Lok, T.S., (1999), *Variational and momentum preservation aspects of smooth particle hydrodynamic formulation,* Comput. Method Appl. M., 180, 97–115.
35- Bonet, J., Kulasegaram, S., (2000), *Correction and stabilization of smooth particle hydrodynamic methods with applications in metal forming simulations,* Int. J. Numer. Meth. Eng., 47, 1189 – 1214.
36- Colagrossi, A. and Landrini, M., (2003), *Numerical simulation of interfacial flows by Smoothed Particle Hydrodynamics,* J. Comput. Phys., 191,448–475.
37- Dilts, G. A.,(1999), *Moving-LeastSquares-Particle Hydrodynamics I. Consistency and stability,* Int. J. Numer. Meth. Eng., 44, 1115–1155.
38- Koshizuka S, Tamako H, Oka Y., (1995), *A particle method for incompressible viscous flow with fluid fragmentation,* J. Comput. Fluid D., 4, 29–46.
39- Monaghan, J. J. and Kos, A., (1999), *Solitary Waves on a Cretan Beach,* J. Waterw. Port Coast. Ocean Eng., 125: 145-154.
40- Rogers, B.D., Dalrymple, R.A., (2008), *SPH modeling of tsunami waves*: Advances in coastal and ocean engineering, Advanced Numerical Models for Tsunami Waves and Runup, Vol. 10.World Scientific.
41- Gomez-Gesteira, M., Cerqueiro, D., Crespo, C., Dalrymple, R.A., (2005), *Green water overtopping analyzed with a SPH model,* Ocean Eng., 32, 223–238.
42- Battjes, J.A.,(1974), *Surf similarity*, 14th Coast. Eng. Conf., ASCE, pp. 466– 480.
43- Ketabdari, M. J., Roozbahani, A. N.,(2013), *Numerical Simulation of Plunging Wave Breaking by the Weakly Compressible Smoothed Particle Hydrodynamic Method,* J. Appl. Mech. Tech. Phys., Vol. 54,No. 3, p p. 477– 486.
44- Vinje, T., Brevig, P., (1981), *Numerical Simulation of Breaking Waves*, J. Advance Water Resources 4, 77‑82.
45- Mahmoudi, A., Hakimzadeh, H. and Ketabdari, M.J., (2014), *Numerical Simulation of Non-Reflected Wave in a Tank Using WCSPH Method,* Proceedings of 11th International Conference on Coasts, Ports & Marine Structures, ICOPMAS.
46- Xu, R., (2010), *An improved incompressible smoothed particle hydrodynamics method and its application in free-surface simulations,* PhD Dissertation, University of Manchester, UK.
47- Liu, S.X., Wang, X.T., Li, M.G., Guo, M.Y., (2003), *Active absorption wave maker system for irregular waves,* China Ocean Engineering, Vol 17, No 2, pp 203-214.